Iron distribution in silicon after solar cell processing: Synchrotron analysis and predictive modeling

D. P. Fenning,[1,a)] J. Hofstetter,[2] M. I. Bertoni,[1,b)] S. Hudelson,[1,b)] M. Rinio,[3] J. F. Lelièvre,[4] B. Lai,[5] C. del Cañizo,[2] and T. Buonassisi[1]

[1]*Massachusetts Institute of Technology, Cambridge, Massachusetts 02139, USA*
[2]*Instituto de Energía Solar, Universidad Politécnica de Madrid, 28040 Madrid, Spain*
[3]*Laboratory and Service Center, Fraunhofer Institute for Solar Energy Systems (ISE), 45884 Gelsenkirchen, Germany*
[4]*Centro de Tecnología del Silicio Solar (CENTESIL), 28905 Getafe, Spain*
[5]*Advanced Photon Source, Argonne National Laboratory, Argonne, Illinois 60439, USA*

(Received 14 October 2010; accepted 20 March 2011; published online 20 April 2011)

The evolution during silicon solar cell processing of performance-limiting iron impurities is investigated with synchrotron-based x-ray fluorescence microscopy. We find that during industrial phosphorus diffusion, bulk precipitate dissolution is incomplete in wafers with high metal content, specifically ingot border material. Postdiffusion low-temperature annealing is not found to alter appreciably the size or spatial distribution of $FeSi_2$ precipitates, although cell efficiency improves due to a decrease in iron interstitial concentration. Gettering simulations successfully model experiment results and suggest the efficacy of high- and low-temperature processing to reduce both precipitated and interstitial iron concentrations, respectively. *© 2011 American Institute of Physics*. [doi:10.1063/1.3575583]

Material defect interactions govern the performance of many emerging energy technologies, including electrochemical, thermoelectric, and photovoltaic devices. In particular, iron impurities are known to have a strong negative influence on minority carrier lifetime in crystalline silicon.[1] The impact of iron contamination depends on its chemical state and spatial distribution, which in turn depend on processing conditions.[2,3] Herein, we use our recently developed "impurities-to-efficiency" (I2E) kinetics simulator,[4] corroborated by synchrotron-based x-ray fluorescence microscopy (μ-XRF), to elucidate how phosphorus diffusion and postdiffusion low-temperature annealing (LTA) determine iron distribution and device performance.

Three adjacent wafers, of thickness 250 μm and boron-doped resistivity 1 Ω-cm, were selected from the upper part of a corner brick of an industrial, directionally-solidified multicrystalline silicon (mc-Si) ingot used in previous LTA experiments.[5] After saw damage etching, one sample was set aside as-grown (AG). The other two wafers underwent a belt phosphorus diffusion gettering (PDG) process at 900 °C for 6 min followed by a 10 min cooldown, producing a 45–50 $\Omega/\square$ emitter. After PDG, one sample underwent a low-temperature anneal of 60 min at 500 °C with the phosphorus glass still present (P+LTA). Samples of 20×20 mm^2 were cut from the AG, PDG, and P+LTA sister wafers from the deteriorated region influenced by the crucible wall, as evidenced by low local internal quantum efficiency.[5] The same grain boundary in all wafers was selected for μ-XRF analysis. Electron back-scatter diffraction measurements (not shown) indicate that the grain boundary selected is random-angle with a misorientation of 44.5°. Such random-angle grain boundaries exhibit high levels of impurity decoration.[6]

Prior to μ-XRF, all samples were cleaned in a sequence of acetone, ethanol, and isopropanol, followed by cleaning with HCl and HF. μ-XRF measurements were obtained at the Advanced Photon Source beamline 2-ID-D at Argonne National Laboratory using a 10 keV incident x-ray beam with 200 nm full-width half-maximum spot size, taking 325 nm steps. National Institute of Standards and Technology standard reference materials 1832 and 1833 were measured in the same detector geometry to convert fluorescence counts into iron concentrations. After measuring the Fe distribution in the AG sample with μ-XRF, a 5×5 mm^2 piece containing the grain boundary was removed and annealed *in situ* in a high-temperature sample stage[7] to compare the effects of an LTA with no gettering layer present (AG+LTA).

Iron precipitates were detected in all samples by μ-XRF, demonstrating that the thermal budget of the phosphorus diffusion was insufficient to dissolve and getter all metals. Of the other 3*d* transition metals, only copper was detected in the gettered samples by μ-XRF (not shown), but at concentrations roughly an order of magnitude lower than iron. Furthermore, copper is known to have a significantly lower impact on lifetime than iron at the same concentrations.[8,9] It is assumed in the simulations below that iron is the lifetime-limiting defect. Over 100 iron precipitates were analyzed in total. The number of atoms in each iron precipitate, shown in Fig. 1, was calculated from the iron loadings measured by μ-XRF assuming that all precipitates were at the surface. The effective precipitate radius, shown along the right axis of Fig. 1, was then calculated assuming a spherical precipitate of room-temperature $FeSi_2$.

Comparing the samples with LTA in Fig. 1 to the corresponding samples without LTA, we conclude that the 500 °C LTA does not change the iron precipitate size distribution. Furthermore, comparing the AG and AG+LTA data, which show the μ-XRF analysis of the same precipitates before and after an *in situ* LTA, it is also clear that the LTA affects the

[a)]Electronic mail: dfenning@alum.mit.edu.
[b)]Present address: 1366 Technologies, North Lexington, MA 02421, USA.

 © 2011 American Institute of Physics

Author complimentary copy. Redistribution subject to AIP license or copyright, see http://apl.aip.org/apl/copyright.jsp

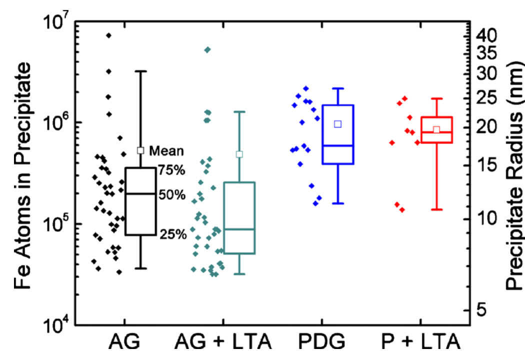

FIG. 1. (Color online) Data points designate individual iron precipitates measured by μ-XRF. The number of atoms per precipitate is shown on the left and converted into an effective precipitate size on the right. The box plots to the right of the data for each sample show the 25th, 50th, and 75th percentiles of precipitate size in that sample. The open box shows the mean precipitate size. LTA is seen to have a minimal effect on the precipitated iron distribution.

density of precipitates minimally. However, there appears to be a decrease in precipitate density and increase in median precipitate size for the samples that underwent the 900 °C P-diffusion process. Along the 35 μm length of the grain boundary observed in each sample, the AG sample contained 1.2 precipitates/μm, and the AG+LTA sample 1.3 precipitates/μm, while the PDG and P+LTA samples showed a decrease in precipitate density to 0.4 precipitates/μm and 0.2 precipitates/μm respectively, with an effective 1/e attenuation length for the fluorescent Fe signal in our μ-XRF setup of 8 μm. If this decrease in density were due to coarsening, a broadening of the precipitate size distribution would be expected[10] but is not seen here. Further, recent results have shown internal gettering has much less of an effect than external gettering during annealing when surface sink layers are present.[11,12] Therefore, the distribution changes after PDG seen in Fig. 1 suggest that dissolution due predominantly to external gettering eliminates smaller precipitates near the emitter. Although the two gettered samples both show the same trend with respect to the ungettered samples, we cannot eliminate the possibility that the variation may be due to wafer-to-wafer variations in local metal impurity concentrations.[13]

To corroborate our experimental observations, we used our I2E diffusion-gettering simulator[4] to solve for the distribution of phosphorus and iron after processing and calculate an effective bulk lifetime. The lifetime and simulated phosphorus profile are then used as inputs for a PC1D device simulation.[14] We simulated the 6 min P-diffusion at 900 °C followed by (a) a 10 min cool down to room temperature and (b) LTA at 500 °C for 60 min. We chose an average AG precipitate radius of 17.5 nm, as measured by μ-XRF, and assumed an initial iron content for the corner wafer of 10^{15} cm^{-3}, typical of border region material.[15,16] We assumed symmetrical gettering to both sides of the wafer. Fe-B pairs were taken to be completely dissociated, and iron precipitates were assumed to be uncharged, causing recombination of carriers at their surfaces. The simulation results for the processed Fe and effective lifetime distributions are shown in Fig. 2.

Due to iron segregation into the 0.3 μm emitter, the simulated bulk Fe content decreased by 35% with respect to the AG concentration for both processes. Beyond the emitter,

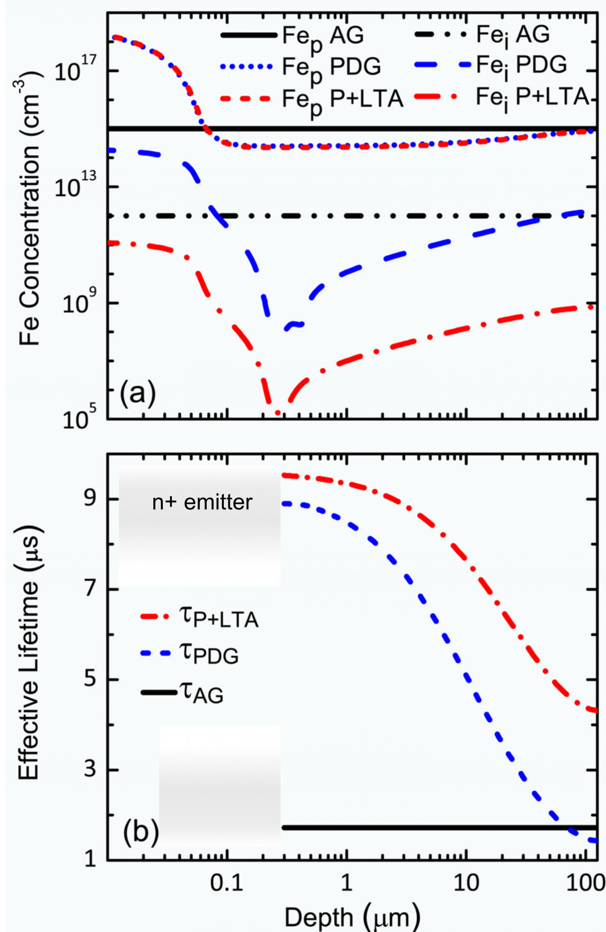

FIG. 2. (Color online) (a) Simulated interstitial, Fe_i, and precipitated, Fe_p, iron profiles after standard PDG and after PDG followed by a 60 min LTA at 500 °C. (b) The resulting effective lifetime in the p-type base for the two different processes is shown. After LTA, the bulk lifetime increases due to the large reduction in iron interstitial population.

both [Fe_p] and [Fe_i] are depleted far into the bulk, as seen in Fig. 2(a), to depths much greater than the 8 μm information depth of the μ-XRF setup. Thus, returning to Fig. 1, the larger precipitate size seen in the PDG-processed samples could be a result of our high sensitivity to large precipitates in or near the heavily-segregated emitter, while the low measured density of precipitates in the PDG samples may reflect the shrinking of many precipitates below detection limits in the iron-poor region just beyond the emitter.

After the standard P-diffusion, the simulated [Fe_i], when averaged over the entire bulk, increased slightly with respect to the AG [Fe_i] due to bulk precipitate dissolution [increase seen at depths greater than 60 μm in Fig. 2(a)], which may explain the degradation of certain material types during high temperature processing.[17] When P-diffusion is followed by LTA, the [Fe_i] decreased over three orders of magnitude. The reduction in [Fe_i] during LTA led to an increase in bulk lifetime, as seen in Fig. 2(b). After LTA, the effective lifetime is dominated by the large amount of iron that remains as recombination-active precipitates.

Using the simulated bulk lifetime and phosphorus profiles, we simulated a device in PC1D using typical parameters of a specific series resistance of 0.8 Ω-cm^2, a specific shunt resistance of 10^3 Ω-cm^2, a front surface recombination velocity of 10^5 cm/s, and a back surface recombination

Author complimentary copy. Redistribution subject to AIP license or copyright, see http://apl.aip.org/apl/copyright.jsp

TABLE I. Experimental and simulated solar cell characteristics for the PDG and P+LTA processes.

Treatment	PDG	P+LTA
Experimental efficiency (%)	14.5[a]	15.2[a]
Simulated efficiency (%)	14.2	15.1
Short circuit current density (mA/cm^2)	31.0	32.4
Open circuit voltage (mV)	592	602

[a]Reference 5.

velocity of 10^3 cm/s. Simulation results for the two processes and the corresponding experimental efficiencies[5] are shown in Table I.

Excellent agreement is observed with the experimental data: ≥0.7% absolute higher solar cell efficiency was both simulated and measured for cells from border regions processed with LTA. The predicted change in the lifetime after LTA due to lower [Fe_i] fully explains the efficiency improvement that is observed experimentally. The combined modeling of lifetime improvement due to [Fe_i] reduction and experimental data on iron precipitates indicate that LTA acts on Fe_i with little effect on precipitated iron.

The removal of precipitated iron in such highly contaminated materials is severely kinetically-limited, since the bulk iron concentration is above the limit of solid solubility. Alternative processing will be required to further improve cell quality from ingot edge regions. To enhance precipitate dissolution, short plateaus at higher temperatures must be considered, followed by an extended, variable-temperature cool down to drive segregation to the emitter in a process similar to that considered by Plekhanov *et al.*[18] and Seibt *et al.*.[19]

To summarize, we observe that a standard PDG process incompletely dissolves precipitated metals in mc-Si that contains high AG metal concentrations. The addition of a low-temperature anneal does not change the precipitated iron distribution significantly, as shown by μ-XRF analysis and simulations. Instead, simulations indicate that the improvement in device efficiency after a LTA can be fully explained by a sharp decrease in interstitial iron concentration due to an enhanced segregation gettering to the P-diffused layer. With confirmation that the I2E model closely predicts the performance of experimental cells, the prospect of simulation-guided process optimization appears within reach for silicon solar cells.

This work was supported by the U.S. Department of Energy, Contract No. DE-FG36-09GO1900, the MIT-Spain/La Cambra de Barcelona Seed Fund, and the Spanish Ministerio de Ciencia e Innovación through Thincells Project No. TEC2008-06798-C03-02. D. P. Fenning and S. Hudelson acknowledge the support of the NSF Graduate Research Fellowship. Use of the Advanced Photon Source at Argonne National Laboratory was supported by the U. S. Department of Energy under Contract No. DE-AC02-06CH11357.

[1]G. Coletti, R. Kvande, V. D. Mihailetchi, L. J. Geerligs, L. Arnberg, and E. J. Øvrelid, J. Appl. Phys. **104**, 104913 (2008).
[2]M. D. Pickett and T. Buonassisi, Appl. Phys. Lett. **92**, 122103 (2008).
[3]P. Manshanden and L. J. Geerligs, Sol. Energy Mater. Sol. Cells **90**, 998 (2006).
[4]J. Hofstetter, D. P. Fenning, M. I. Bertoni, J. F. Lelièvre, C. del Cañizo, and T. Buonassisi, Prog. Photovoltaics (to be published).
[5]M. Rinio, A. Yodyunyong, S. Keipert-Colberg, Y. P. B. Mouafi, D. Borchert, and A. Montesdeoca-Santana, Prog. Photovoltaics **19**, 165 (2011).
[6]T. Buonassisi, A. A. Istratov, M. D. Pickett, M. A. Marcus, T. F. Ciszek, and E. R. Weber, Appl. Phys. Lett. **89**, 042102 (2006).
[7]S. Hudelson, B. K. Newman, S. Bernardis, D. P. Fenning, M. I. Bertoni, M. A. Marcus, S. C. Fakra, B. Lai, and T. Buonassisi, Adv. Mater. (Weinheim, Ger.) **22**, 3948 (2010).
[8]J. Hofstetter, J. F. Lelièvre, C. del Cañizo, and A. Luque, Mater. Sci. Eng., B **159–160**, 299 (2009).
[9]J. R. Davis, Jr., A. Rohatgi, R. H. Hopkins, P. D. Blais, P. Rai-Choudhury, J. R. McCormick, and H. C. Mollenkopf, IEEE Trans. Electron Devices **27**, 677 (1980).
[10]X. W. Lin, J. Washburn, Z. Liliental-Weber, and H. Bernas, J. Appl. Phys. **75**, 4686 (1994).
[11]J. Hofstetter, J. F. Lelièvre, C. del Cañizo, and A. Luque, Solid State Phenom. **156–158**, 387 (2010).
[12]M. Rinio, A. Yodyunyong, M. Pirker, C. Zhang, D. Günther, P. Botchak, S. Keipert, D. Borchert, M. Heuer, and A. Montesdeoca-Santana, *Proceedings of the 24th EU PVSEC* (WIP, Munich, 2009), p. 1816.
[13]A. Zuschlag, S. Ohl, J. Bernhard, H. Morhenn, J. Ebser, J. Junge, S. Seren, and G. Hahn, *Proceedings of the 35th IEEE Photovoltaic Specialists Conference* (IEEE, New York, 2010).
[14]D. A. Clugston and P. A. Basore, *Proceedings of the 26th IEEE Photovoltaic Specialists Conference* (IEEE, New York, 1997), p. 207.
[15]D. Macdonald, A. Cuevas, A. Kinomura, Y. Nakano, and L. J. Geerligs, J. Appl. Phys. **97**, 033523 (2005).
[16]T. U. Nærland, L. Arnberg, and A. Holt, Prog. Photovoltaics **17**, 289 (2009).
[17]L. J. Geerligs, Y. Komatsu, I. Röver, K. Wambach, I. Yamaga, and T. Saitoh, J. Appl. Phys. **102**, 093702 (2007).
[18]P. S. Plekhanov, R. Gafiteanu, U. M. Gösele, and T. Y. Tan, J. Appl. Phys. **86**, 2453 (1999).
[19]M. Seibt, A. Sattler, C. Rudolf, O. Voß, V. Kveder, and W. Schröter, Phys. Status Solidi A **203**, 696 (2006).

Author complimentary copy. Redistribution subject to AIP license or copyright, see http://apl.aip.org/apl/copyright.jsp